Composites Communications 46 (2024) 101832

Contents lists available at ScienceDirect

Composites Communications

journal homepage: www.elsevier.com/locate/coco

Short Communication

UV-induced frontal polymerization for optimized in-situ curing of epoxy resin for excellent tensile and flexural properties

Amirreza Tarafdar [a], Wenhua Lin [a], Ali Naderi [a], Xinlu Wang [b], Kun (Kelvin) Fu [c], Ian D. Hosein [b], Yeqing Wang [a,*]

[a] Department of Mechanical & Aerospace Engineering, Syracuse University, Syracuse, NY, 13244, USA
[b] Department of Biomedical & Chemical Engineering, Syracuse University, Syracuse, NY, 13244, USA
[c] Department of Mechanical Engineering, University of Delaware, Newark, DE, 19716, USA

ARTICLE INFO

Keywords:
Frontal polymerization
Epoxy resin
Sustainable manufacturing
Out-of-oven curing
Mechanical properties

ABSTRACT

UV-induced frontal polymerization is an emergent rapid curing method for thermoset resin and its fiber composites which features the generation of a self-sustaining front that propagates within the entire material. This is different from using the commercially available UV curable resin which prohibited the curing of thermoset composites with opaque fibers (*e.g.,* carbon fiber) due to the UV light being blocked by the fibers. In this study, we experimentally demonstrate that using the UV-induced frontal polymerization allows us to reduce the curing time of a standard tensile specimen of epoxy resin from traditionally 15 h using the oven curing method to only less than 1.5 min. The frontal polymerized epoxy specimens showed comparable and even superior tensile and flexural properties when compared to the traditional oven cured specimens. Moreover, we experimentally investigated the influence of the weight content of the photoinitiator, the UV light intensity, and the specimen geometry on the characteristics of the frontal polymerization process (*i.e.,* front temperature, front velocity, and degree of cure) and the resulting tensile and flexural properties. The results and discussions are expected to provide guidance in scaling up this UV-induced frontal polymerization technique for the sustainable and additive manufacturing and repair of thermoset resin and its fiber composites.

1. Introduction

Thermoset resin and thermoset resin-based fiber reinforced composites are increasingly used in a variety of industries, including aerospace, automotive, marine and energy due to their significant weight saving capability and outstanding properties. Traditional manufacturing and repair of thermoset and thermoset-based fiber composites require prolonged curing duration and intensive energy consumption for cross-linking and consolidation, which are typically achieved through the thermal curing method using an oven or an autoclave. For example, the complete cure cycle of the Solvay CYCOM 977-2 epoxy resin requires about 10 h in an autoclave [1]. Such a prolonged curing time has significantly hindered the additive manufacturing and repair of thermoset resin and its fiber composites. Nowadays, with the growing demand for sustainable and additive manufacturing, innovative out-of-oven/autoclave manufacturing techniques for thermoset resin and its fiber composites have been a focus of interest [2–7]. Among which, one of the emergent out-of-oven/autoclave manufacturing techniques is the frontal polymerization (FP) technique. The FP technique features a self-propagating exothermic reaction zone, *i.e.,* a curing front, initiated using a localized triggering mechanism, such as a soldering iron or a UV light, which converts the cold beyond monomer region to a hot-formed polymer [5,8], and allows the curing front to propagate within the entire thermoset monomer even with the presence of opaque fibers, such as carbon fiber and carbon nanotubes. This also distinguishes the FP technique from the commercially available UV curable resin or conventional photopolymer [9–11], which is unable to in-situ cure thermoset composites with opaque fibers due to the UV light being blocked by the opaque fibers from penetrating into the in-depth of the composites. When compared to the conventional autoclave/oven curing method, the FP is capable of reducing the curing time from traditionally several hours to only a few minutes or seconds, which substantially reduces the energy consumption and the associated environment impact [12–14]. The performance of the FP process, including the front temperature and velocity, the degree of cure, and the resulting mechanical properties are highly influenced by the weight content of the

* Corresponding author.
E-mail address: ywang261@syr.edu (Y. Wang).

https://doi.org/10.1016/j.coco.2024.101832
Received 6 December 2023; Received in revised form 22 January 2024; Accepted 22 January 2024
Available online 28 January 2024

initiators (*i.e.,* photoinitiator, thermal co-initiator) in relative to the monomer [15,16] as well as the microstructure and architecture of the fiber reinforcements (for thermoset resin-based fiber composites) [17,18].

Among thermoset resin systems, the dicyclopentadiene (DCPD) acrylate system, due to their robust activities and low exothermicities, lend themselves naturally to the FP technique, which have been extensively studied [19–21]. Despite that several recent studies have demonstrated the success of using FP to polymerize fiber reinforced composites with DCPD resin, the use of the DCPD resin in the current industrial applications is still limited due to its short pot life of a few hours [5,22]. Another thermoset resin system is known as the epoxy-based resin. When compared to the DCPD acrylate resin, the epoxy-based resins are extensively utilized in the fabrication of plastics and fiber reinforced composites in the industry [23–25]. Although less widely studied, this type of monomer can also be polymerized using the FP technique, more specifically, using the radical-induced cationic frontal polymerization (RICFP) technique [26]. This method provides a longer resin pot life along with having the benefit of this resin system being more widely used in the industry, in contrast with the DCPD acrylate resin. The RICFP process of the epoxy resin features the unique use of two separate initiator systems (*i.e.,* photoinitiator and thermal co-initiator), which stabilizes the resin mixture and allows it to remain intact for about a month in a dark environment at an ambient temperature of up to 50 °C [27]. A few recent studies have investigated the RICFP process of the epoxy-based carbon fiber composites. For example, Tran et al. [28] investigated the mechanical properties of carbon fiber reinforced polymer (CFRP) composites fabricated by the RICFP process using bisphenol A diglycidyl ether (BADGE), diaryliodonium tetrakis (perfluoro-tert-butoxy) aluminate, and benzopinacol as the monomer, the photoinitiator, and the thermal co-initiator, respectively. They achieved a fiber volume fraction of 35 %. The mechanical properties of the composites were found to be comparable to those manufactured using the traditional thermal curing method.

As aforementioned, the performance of the FP process and the resulting mechanical properties of the thermoset resin and its fiber composites are highly influenced by the weight contents of initiators in relative to the monomer resin. They are also affected by the triggering source, such as the heat from the soldering iron or the UV light intensity. Moreover, they are impacted by the geometry and the boundary condition of the specimens. These factors essentially control the generation of the exothermic heat as well as the heat conduction within the epoxy and the heat exchange with the ambient environment. Although existing studies have demonstrated the successful fabrication of thermoset resin and its fiber composites using the FP process with various single- or dual-initiator systems, the fundamental effects of the initiator concentration, triggering source, and the specimen geometry on the FP process and the resulting mechanical properties still remain unclear. The current study aims to fill this knowledge gap and investigate these fundamental effects on the UV light-induced FP process of the epoxy resin and the resulting mechanical properties. Results from this study not only show that the frontal polymerized specimens compare favorably with those fabricated using the traditional oven curing method, but also are expected to provide guidance and insights into the scale-up of the FP technology for the sustainable and additive manufacturing and repair of epoxy resin and its fiber composites.

2. Materials, UV-induced frontal polymerization, and traditional thermal polymerization

The monomer of the epoxy resin used in this study is: (3,4-epoxycyclohexane)-methyl-3,4-epoxycyclohexyl carboxylate (ECC, MilliporeSigma, USA). To enable the radical induced cationic frontal polymerization (RICFP) of the epoxy monomer, p-(octyloxyphenyl) phenyl iodonium hexafluorostibate (IOC-8 SbF6, AmBeed, USA) and benzopinacol (AAblocks, USA) were used as the photo-initiator (PI), and the thermal-initiator (TI), respectively. The weight contents of the TI was fixed at 1 wt% in relative to the weight of the epoxy monomer, as suggested by Ref. [5]. The weight ratio of the PI was varied between 0.1 wt% and 0.5 wt%. For each specific PI content level, three replicate specimens were fabricated to account for the statistical variation. The mixture was poured into a silicone elastomer mold, with a cavity of specimens used for tensile and flexural tests (see Fig. 1). Note that choosing the silicone elastomer to fabricate the molds is important, because silicone has a low thermal conductivity, which could minimize the heat loss in the FP process. The front was initiated using an Omni-Cure S2000 Spot UV Curing System. The UV light was immediately removed once the front has formed and started propagating. A FLIR One Pro thermal camera was placed on top of the mold and used to record the evolution of the temperature field in the FP process.

On the other hand, to enable the comparison between the UV-induced FP and the traditional oven curing method, baseline epoxy resin specimens were fabricated using the same epoxy resin monomer with the cycloaliphatic 4-methylhexahydrophthalic anhydride (MHHPA) and Tertiary amine N,N-dimethylbenzylamine (DMBA) as the thermal curing agent and catalyst, respectively.

The details of specimen fabrication using the UV-induced frontal polymerization (FP) technique and using the traditional oven curing method, as well as the experimental details regarding the characterization of the temperature and the degree of cure and characterizations of the tensile and flexural properties can be referred in Supporting **Information**.

3. Results & discussion

3.1. Effect of weight content of photoinitiator (PI) and the UV light intensity

Fig. 2 shows the evolution of the temperature field in the FP process recorded using a FLIR thermal camera in two representative epoxy resin specimens, one fabricated in the mold with a flat beam shaped cavity (referred as the “flat beam specimen”) and the other fabricated in the mold with a dog-bone shaped cavity (referred as the “dog-bone specimen”), both with a PI weight content of 0.3 wt%. Real-time spot measurements were used to capture the temperature, without manipulating the acquired data from the FLIR thermal tools. Also, the white area represents the highest temperature zone, transitioning to red to indicate decreasing temperatures away from the front. The corresponding videos can be found in the **Supplementary Data**. The evolution of the temperature field was analyzed to obtain the initiation duration, total curing time, the front temperature, and the average front velocity. The detailed methods for such analyses are documented in the Supporting **Information**.

3.1.1. Initiation time, total curing time, front temperature, and front velocity

To study the effect of the UV light intensity, two UV intensity levels were used, one with 42 mW/cm^2, which is 15 % of the maximum UV light power (hereafter “15 % UV”) and the other with 82 mW/cm^2, which represents 25 % of the maximum UV power (hereafter “25 % UV”). In our early experiments, we discovered that the UV light intensity is key to controlling side reactions (*e.g.,* carboxylation) in UV-induced frontal polymerization. We observed bubble formation on specimen surfaces exposed to air, a result of high UV intensity levels. By reducing the UV intensity to 25 % and 15 % of its maximum, we initiated polymerization while substantially removing bubbles and oxidation. Yet, with 0.4 % and 0.5 % wt% PI, bubbles still formed in the flat beam specimens, indicating a link between PI concentration, UV intensity, and side reactions.

Three levels of PI weight content were investigated at each UV light intensity level. Specifically, under 15 % UV, specimens were prepared using PI contents of 0.3 wt%, 0.4 wt%, and 0.5 wt%, while under 25 %

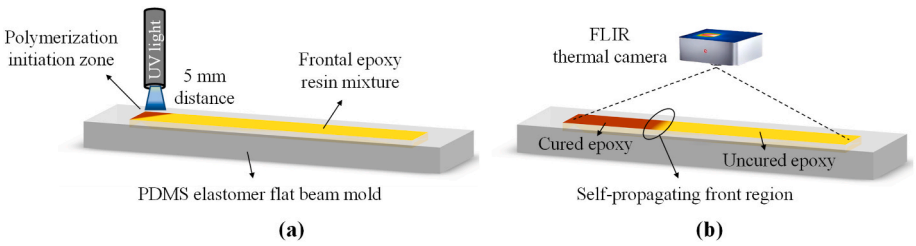

Fig. 1. Schematic of the UV light-induced frontal polymerization of epoxy resin in a PDMS elastomer mold with a flat beam cavity: **(a)** the initiation of the front by applying a spot UV light and **(b)** the propagation of the front during the process recorded using a FLIR thermal camera.

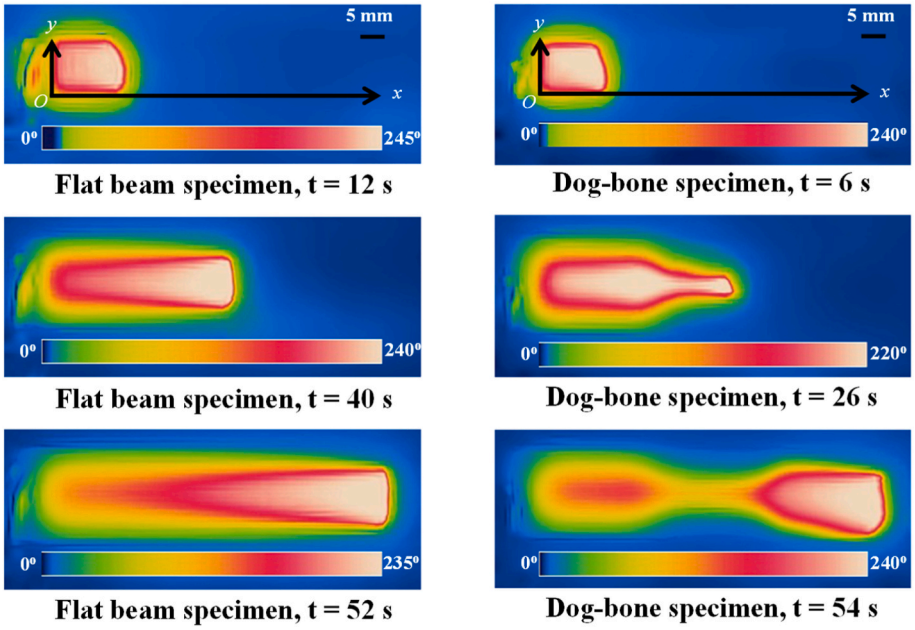

Fig. 2. Evolution of the temperature field (unit in °C) recorded from the top surface of the flat beam specimen (left) and the dog-bone specimen (right) with 0.3 wt% photoinitiator (PI) content under 15 % UV condition (42 mW/cm^2).

UV, specimens were prepared using 0.2 wt%, 0.3 wt%, and 0.4 wt%. Note that the choice of the three PI content levels at the two UV conditions do not exactly overlap. This is because the 15 % UV is too weak to result in a meaningful degree of cure for specimens with a PI of 0.2 wt%, under which, although the front can still be initiated, the epoxy is far from being fully cured after the FP process. On the other hand, the 25 % UV light is too high for specimens with 0.5 wt% PI, which has resulted in the charring of the specimen after the FP process.

Fig. 3(a) shows the influence of the PI weight content and the UV light intensity on the initiation duration and total curing time of the flat beam specimens (*i.e.,* fabricated using the elastomer mold with a cavity of a flat beam shape). Results show that both the initiation duration and total curing time decrease with the increase of the PI weight content. As the PI weight content increases, the reductions in the initiation duration and total curing time becomes more significant. Such an effect is true for specimens at both 25 % UV and 15 % UV intensity levels. Specifically, at 25 % UV, the reduction in the initiation duration is 12 % (from 8.3 s to 7.3 s) when the PI content increases from 0.2 wt% to 0.3 wt%, whereas such a reduction increases to 55 % (from 7.3 s to 3.3 s) when the PI increases from 0.3 wt% to 0.4 wt%. Similarly, the reductions in the total curing time are 10 % (from 74.3 s to 66.7 s) as PI increases from 0.2 wt% to 0.3 wt% and 37 % (from 66.7 s to 42.0 s) as the PI increases from 0.3 wt% to 0.4 wt%, respectively. Moreover, the influence of the UV light intensity can be checked by comparing the 0.3 wt% and 0.4 wt% cases under the 25 % and 15 % UV conditions. As one can see, the UV light intensity does not show a significant effect at a PI content of 0.3 wt%. However, when the PI content increases to 0.4 wt%, a higher UV light intensity significantly reduces the initiation duration and the total curing time. Specifically, the initiation duration decreased by 55 % while the total curing time decreased by 17 %. Our results suggest that the generation of the exothermic heat is highly dependent on the coupling between the UV intensity and the PI weight content. Increasing the PI weight content and UV intensity generally both increase the exothermic heating. Both effects are more pronounced at a higher PI = content of above 0.3 wt%. Such a finding is also evidenced in the recorded front temperature as discussed below.

To further illustrate the effect of the PI weight content and the UV light intensity on the generation of the exothermic heat, Fig. 3(b) provides a comparison of the front temperature *vs.* PI weight content at both 25 % UV and 15 % UV conditions. Similar to the initiation duration and total curing time, the front temperature generally increases as the PI content and the UV light intensity increases. Moreover, at a higher PI content of above 0.3 wt%, such an increase in the front temperature becomes more significant as the PI content and UV intensity increase. Specifically, under the 25 % UV condition, the front temperature increases from 242 °C to 247 °C as the PI content increases from 0.2 wt% to 0.3 wt% while such an increase further rises from 247 °C to 263 °C as the PI increases from 0.3 wt% to 0.4 wt%. Under the 15 % UV condition, the front temperature follows an approximate linear increase from 248 °C to 259 °C and 268 °C as the PI increases from 0.3 wt% to 0.4 wt% and 0.5 wt%. Such a linear increase relation correlates well with the linear reduction relation of the total curing time *vs.* PI content as

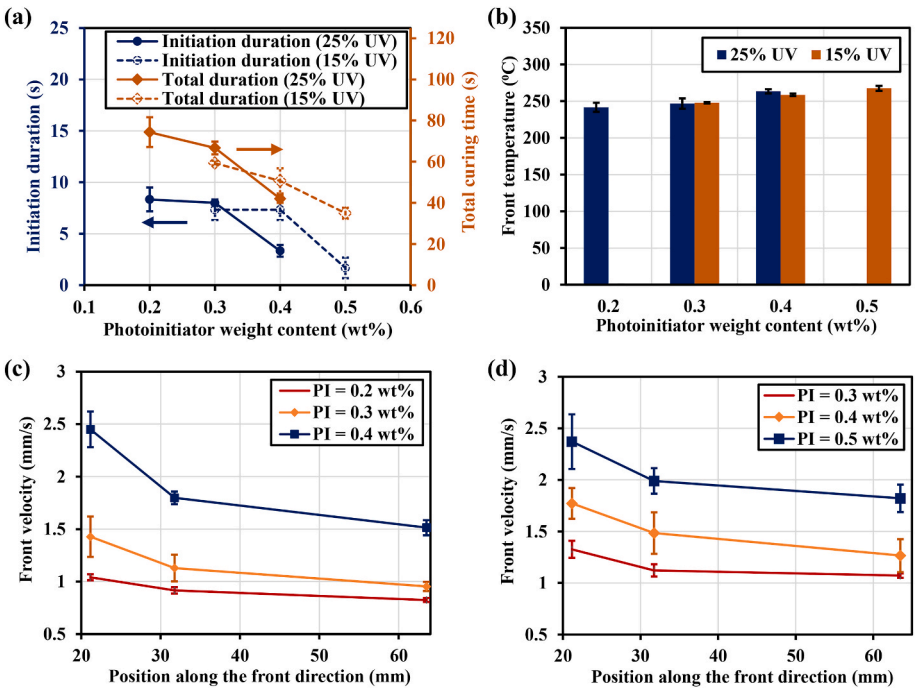

Fig. 3. The influence of PI weight content and UV light intensity on the **(a)** initiation duration, total curing time, and **(b)** the front temperature. The effect of the PI content on the average front velocity along the front propagating path under **(c)** 25 % UV (82 mW/cm^2) and **(d)** 15 % UV (42 mW/cm^2) UV conditions.

depicted in Fig. 3(a). This suggests that the total curing time during FP process is highly dominated by the generation of the exothermic heat. When comparing the front temperature under the 15 % UV and 25 % UV conditions, it can be seen that the front temperature is not much affected by the increase of the UV intensity at 0.3 wt%, however, it experienced a large reduction from 263 °C to 259 °C at 0.4 wt%. Such a behavior also agrees with the findings associated with the initiation duration and total curing time as presented in Fig. 3(a).

Fig. 3(c) and (d) show the average front velocity measured at three prescribed locations in the flat beam specimen (x=21.0 mm, 32.0 mm, and 63.5 mm) under the 25 % UV and 15 % UV conditions, respectively. A similar decreasing trend can be observed under both conditions as the front propagates along the path. The rate of reduction becomes milder as the front propagates along the path and as the PI content decreases. For example, under 25 % UV and at 0.4 wt% PI (in Fig. 3 (c)), the front velocity experienced a 27 % reduction from 2.45 to 1.80 mm/s as the front propagates from x=21.0 to 32.0 mm. As the front further propagates to 63.5 mm, the percentage drop in the front velocity has reduced to 16 %. When the PI decreased from 0.4 wt% to 0.2 wt%, the percentage drop reduced from 65 % to 12 % as the front propagates from x=21.0 to 32.0 mm, and reduced from 16 % to 11 % as the front further propagates to 63.5 mm. The same effect has been observed under the 15 % UV condition as shown in Fig. 3(d). Comparing the front velocity under the same PI content shows that the front velocity increases generally as the UV intensity increases. Specifically, the front velocity at x=21.0 mm in the specimen with 0.4 wt% PI under 25 % UV condition (2.45 mm/s) is 37 % higher than that of under the 15 % UV (1.77 mm/s). In addition, it was observed that the reduction in the front velocity under the 25 % UV condition is more significant when compared to that under the 15 % UV condition. For example, the reduction in the front velocity is 26 % under the 25 % UV light as the front propagates from x=21.0 to 32.0 mm, while the reduction is only 16 % under the 15 % UV light. The same phenomenon has also been observed in the specimen with 0.3 wt% PI. Overall, it can be seen that the rate of reduction in the front velocity (*i.e.*, the slope of the front velocity) decreases as the front propagates in the specimen. Also, the rate of reduction under 25 % UV light is more significant than that under 15 % UV light. Physically, this indicates that the rate of reduction in the front velocity in the FP process is highly dictated by the PI weight content (as further discussed in the next section). As the PI content increases, the rate of reduction increases. Moreover, the rate of the cure reduces as it propagates along the path due to the heat dissipation along the path caused by the heat conduction within the epoxy as well as the heat radiation and convection between the epoxy and the ambient environment.

3.1.2. *Degree of cure*

Fig. 4(a) shows a visual comparison of the specimens cured under 15 % UV (left) and 25 % UV (right) conditions. Our results in Fig. 4(b) show that the degree of cure of the epoxy specimens increases as the PI weight content increases. Specifically, under the 25 % UV condition, the degree of cure increased from 76 % to 89 % and 95 % as the PI content increases from 0.2 wt% to 0.3 wt% and 0.4 wt%, respectively. The same trend is also observed in specimens under the 15 % UV condition. Specifically, the degree of cure improved from 74 % to 84 % and 85 % as the PI content increases from 0.3 wt% to 0.4 wt% and 0.5 wt%. Furthermore, at the same PI content level, the degree of cure is significantly higher in specimens under the 25 % UV condition than in those under the 15 % UV condition.

The results indicate that increasing the UV intensity and the PI weight content are both beneficial in improving the degree of cure of the epoxy resin. However, although increasing the UV intensity helps improve the degree of cure, we observed that it could cause an adverse effect of substantially increasing the porosity due to the higher exothermic heat produced and the side reactions [29–31] in the specimens, as shown in Fig. 4(a). This is also true for increasing the PI weight content. Our porosity analysis (see in the Supporting **Information**) shows that the porosity escalated from 0.1 % to 0.2 % as the UV intensity increased from 15 % to 25 % at a constant PI content of 0.3 wt% for flat beam specimens. Moreover, the porosity rose from 0.2 % to 1.0 % as the PI content increased from 0.3 wt% to 0.4 wt% under 25 % UV. A similar trend was also observed in dog-bone specimens. Additionally, due to the smaller total volume of the dog-bone specimens as opposed to the flat beam specimens, the exothermic heat produced is relatively lower, and hence, it can be visually observed that the increase in the porosity in

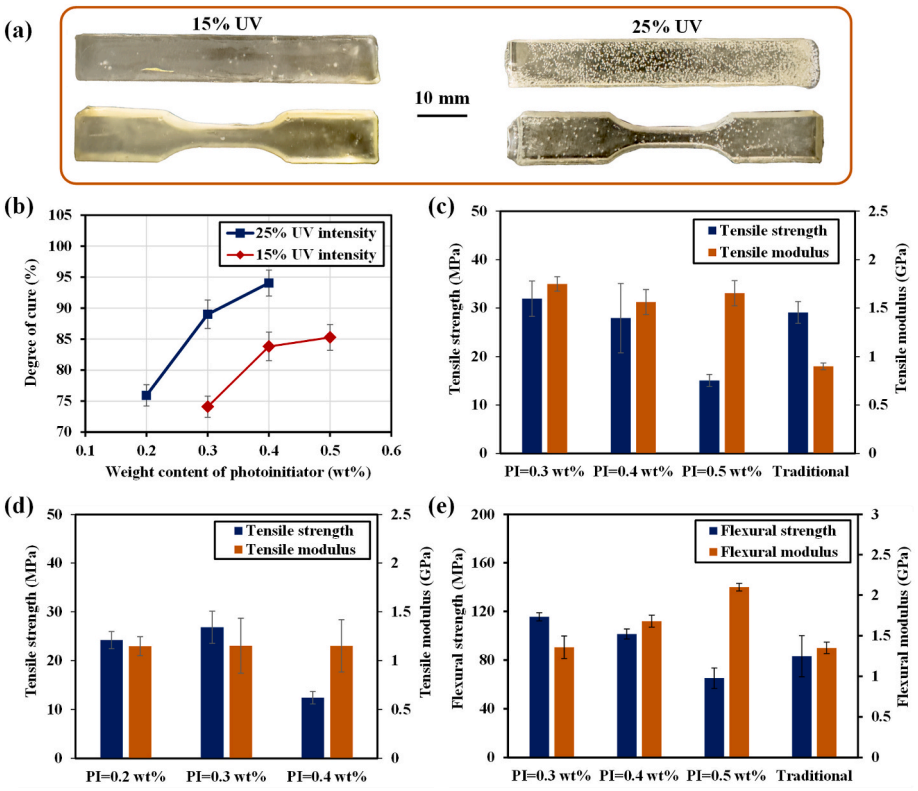

Fig. 4. (a) A visual comparison of the epoxy resin specimens fabricated in the flat beam mold and the dog-bone mold containing 0.3 wt% PI content cured under 15 % UV and 25 % UV conditions. **(b)** The degree of cure of specimens cured in the flat beam mold under 25 % UV and 15 % UV conditions at varying weight contents of photoinitiator (PI). Tensile strength and modulus of the specimens fabricated **(c)** under 15 % UV and their comparisons with specimens fabricated using the traditional oven curing method (denoted as "Traditional") and **(d)** under 25 % UV conditions. **(e)** The influence of the PI content on the flexural strength and modulus under 15 % UV condition and the comparison with the traditionally oven-cured specimens.

dog-bone specimens is much less significant when compared to that in flat beam specimens as the UV intensity increases from 15 % to 25 %. Therefore, although improving the UV light helps to increase the degree of the cure, it adversely increases the porosity. The consequence is that the mechanical properties are compromised, as will be discussed in the following section.

3.1.3. *Tensile and flexural properties*

The influence of the PI weight content and the UV light intensity on the tensile properties are plotted in Fig. 4(c) and (d). A general finding is that increasing the PI weight content decreases the tensile strength. The reduction in the tensile strength becomes more significant at higher PI contents of above 0.3 wt%, under both UV conditions. Specifically, under 15 % UV, the tensile strength decreased by 13 % and 50 % when the PI content increased from 0.3 wt% to 0.4 wt% and from 0.4 wt% to 0.5 wt%, respectively. Under 25 % UV, the tensile strength increased by 11 % from 24.1 MPa to 26.8 MPa when the PI increased from 0.2 wt% to 0.3 wt%. Moreover, the tensile strength further dropped by 54 % from 26.8 MPa to 12.4 MPa when the PI increased to 0.4 wt%. Another finding is that the tensile strengths are slightly higher for specimens cured under 15 % UV than those cured under 25 % UV at the same PI content. Specifically, at 0.3 wt% and 0.4 wt%, the tensile strengths are 32.0 MPa and 27.9 MPa under 15 % UV, respectively, as opposed to 26.8 MPa and 12.4 MPa under 25 % UV. Additionally, in Fig. 4(c), when the frontal specimens are compared to specimens cured using the traditional oven curing method (denoted as "Traditional"), it can be seen that the strengths of the frontal specimens are comparable (28.0 MPa at 0.4 wt%) and even higher (32.0 MPa at 0.3 wt%) than the tensile strength of the traditional specimen (29.0 MPa). When the PI increases to 0.5 wt%, the tensile strength (13.9 MPa) becomes much lower than the strength of the traditional specimen. These findings suggest that increasing the PI weight content or the UV light intensity could compromise the tensile strength due to the increased temperature, which inevitably leads to the production of side reactions and a higher porosity in the FP process.

Generally, our study indicates that the ECC epoxy resin's mechanical properties, when subjected to either conventional thermal oven curing or frontal polymerization, may not match the performance of other thermoset resin such as DCPD resin cured frontally. Specifically, the tensile strength and Young's modulus of either thermally or frontally cured neat DCPD specimens ranges from 20 to 50 MPa and 0.4-2 GPa are potentially higher than those of ECC or Badge thermoset resin, respectively. This comparison underscores the distinct benefits and constraints associated with different resin types across diverse curing methodologies.

Unlike the tensile strength which shows a clear decreasing trend with the increase of the PI content, the tensile modulus is less impacted by the PI weight content and does not show a clear trend, as shown in Fig. 4(c) and (d). The average tensile modulus of frontal specimens is 1.7 GPa and 1.2 GPa under 15 % UV and 25 % UV, respectively. Hence, the modulus is on average 42 % higher in specimens under the 15 % UV condition. Moreover, when compared to the modulus of the traditional specimen (0.9 GPa), the average modulus of frontal specimens is 89 % and 33 % higher under 15 % UV and 25 % UV conditions, respectively.

The flexural properties of the epoxy specimens fabricated using the FP method are shown in Fig. 4(e). Note that the flexural tests were only conducted with specimens that are fabricated under the 15 % UV condition due to its better performance as discussed in the results for tensile properties. Similar to the tensile strength, the flexural strength decreases as the PI content increases. Specifically, the flexural strengths decreased from 115.5 MPa to 101.5 MPa and 65.1 MPa when the PI increases from 0.3 wt% to 0.4 wt% and 0.5 wt%, rendering a percentage decrease of 12

% and 36 %, respectively. When compared to the traditional specimen (83.2 MPa), the flexural strengths of the frontal specimens at 0.3 wt% and 0.4 wt% are 38 % and 22 % higher, respectively. When the PI increases to 0.5 wt%, the flexural strength becomes lower than that of the traditional specimen, which is likely caused by the polymer degradation and the status of being mushy right after the polymerization process as a result of the high temperature (as shown in Fig. 4(a)). Unlike the flexural strength which shows a decreasing trend as the PI content increases, the flexural modulus shows an opposite trend, in which it increases as the PI content increases. Specifically, the average flexural modulus is 1.4 GPa, 1.7 GPa, and 2.1 GPa at PI contents of 0.3 wt%, 0.4 wt%, and 0.5 wt%, respectively. The frontal specimen with 0.3 wt% PI content shows an identical flexural modulus to that of the traditional specimen fabricated using the oven curing method (1.4 GPa), but with a relatively higher standard deviation (*i.e.,* 0.14 *vs.* 0.07), indicating that using the FP method to fabricate the epoxy resin could potentially cause a higher non-uniformity in the flexural modulus. The average flexural modulus of the specimens with 0.4 wt% and 0.5 wt% PI contents are 21 % and 50 % higher than that of the traditional specimen, respectively.

3.2. Effect of the geometry: flat beam vs. dog-bone specimens

As discussed in Section 2.1, to investigate how the geometry affects the FP process, two types of elastomer molds were used, one with a cavity of a flat beam shape and the other with a cavity of a dog-bone shape (*i.e.,* Type V dog-bone shape as suggested in ASTM D638 [32]). We chose to compare the dog-bone shape, a tensile testing standard, with the flat beam shape to assess how changing the cross-sectional area along the front propagating path affects FP characteristics and mechanical properties. This comparison, under constant PI wt% and UV intensity, is crucial for understanding how variations in geometry influence the overall FP characteristics and strength of the samples, providing a baseline guidance for future scale-up studies.

Using the dog-bone shaped mold, as the front propagates from the shoulder into the slender gauge section in the center of the dog-bone, it constricts the front, thereby causing differences in the FP behaviors when compared to those in the flat beam molds. Fig. 2 shows a comparison of the evolution of the temperature field as the front propagates in a flat beam mold *vs.* in a dog-bone mold. In what follows, specimens fabricated in the flat beam mold will be referred as the flat beam specimens while the ones fabricated in the dog-bone mold will be referred as the dog-bone specimens.

3.2.1. Initiation duration, total curing time, front temperature, and front velocity

The experimental results of the initiation duration and total curing time in the dog-bone specimens *vs.* the flat beam specimens at varying PI contents are presented in Fig. 5(a). Our results show that the specimen geometry does not have a significant impact on the initiation time. As shown in Fig. 5(a), similar to the results for flat beam specimens in Fig. 3 (a), the initiation time is not much affected as the PI content increases from 0.3 wt% to 0.4 wt%, however, it experienced a significant drop of 57 % as the PI increases from 0.4 wt% to 0.5 wt%. These initiation durations and the trend are identical to those of the flat beam specimens.

The specimen geometry shows a big influence on the total curing time and the front temperature. Fig. 5(a) and (b) provide the comparison between the flat beam specimens and the dog-bone specimens at varying PI contents for the total curing time and the front temperature. The total curing time in dog-bone specimens shows a decreasing trend as the PI content increases, similar to that in the flat beam specimens. When comparing the two types of specimens, it can be seen that the average total curing time experienced reductions of 10.1 % and 9.2 % in dog-bone specimens at PI contents of 0.3 wt% and 0.4 wt%, respectively. However, as the PI increases to 0.5 wt%, the total curing time in dog-bone specimens becomes higher than that in the flat-beam specimens, highlighting the more significant role that the PI weight content plays, which has led to the generation of a higher exothermic heat in the flat beam specimens, and hence reducing the total curing time.

Although the front temperature shows a similar increasing trend as the PI content increases, the front temperature in the dog-bone specimens is consistently lower than that in the flat beam specimens. This can be explained by the reduced total volume of the epoxy monomer in the dog-bone shaped cavity when compared to that in the flat beam shaped cavity, which resulted in the less total exothermic heat generated. Moreover, it is observed that the difference in the front temperature between the flat beam and the dog-bone specimens decreases as the PI content increases (see Fig. 5(b)). Specifically, the reductions in the dog-bone specimens are 2.0 %, 1.6 %, and 0.6 % at PI contents of 0.3 wt%, 0.4 wt%, and 0.5 wt%, respectively. This implies that both the total volume of the frontal resin and the PI content are important factors that

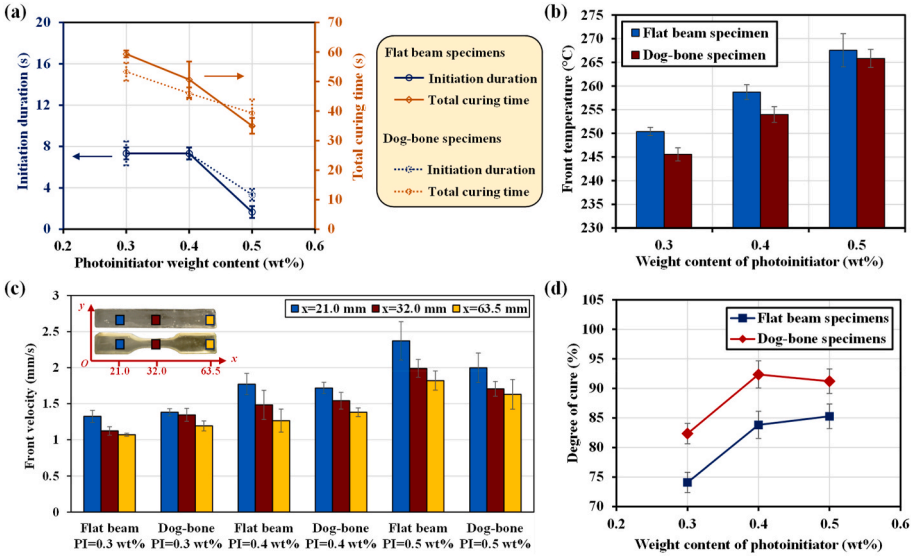

Fig. 5. A comparison of **(a)** the initiation duration and total curing time and **(b)** front temperature in flat beam *vs.* dog-bone specimens. **(c)** Average front velocity in flat beam *vs.* in dog-bone epoxy resin specimens at three prescribed locations (x=21.0 mm, 32.0 mm, and 63.5 mm) fabricated using the frontal polymerization method under 15 % UV condition. **(d)** A comparison of degree of cure for flat beam *vs.* dog-bone epoxy resin specimens at varying PI weight contents fabricated using the frontal polymerization method under the 15 % UV condition.

contribute to the generation of the exothermic heat, in which the PI content plays a more significant role in generating the heat as the PI content increases.

Fig. 5(c) shows a comparison of the average front velocity between the flat beam and dog-bone specimens at three prescribed locations (x=21.0 mm, 32.0 mm, and 63.5 mm, see the insert in Fig. 5(c)) at the three PI weight contents. The first observation is that the average front velocity in dog-bone specimens shows a similar decreasing pattern as in the flat beam specimens. The second observation is that the average front velocity in dog-bone specimens also increases as the PI content increases. Moreover, when compared to the flat beam specimens, the average front velocity increased by 3.8 %, 20.5 %, and 11.2 % at x=21.0 mm, 32.0 mm, and 63.5 mm in the dog-bone specimens, respectively, at a PI of 0.3 wt%. As the PI content increases, the higher average front velocity in the dog-bone specimen is mitigated by the increased total exothermic heat generated in the flat beam specimens. This can be explained by checking the analytic formula for the front velocity based on the cure kinetics model, $V^2 = \left(\frac{Ak}{\rho H_e}\frac{RT_{max}^2}{E}\exp\left(\frac{-E}{RT_{max}}\right)\right)\frac{1}{\varnothing}$ [33], where A, k, E are curing kinetics parameters, R is the gas constant, ρ is the density, H_e is amount of heat generated by the exothermic reaction of the resin, T_{max} is the front temperature, and $\varnothing$ is a parameter associated with the curing kinetics model. As the equation shows, the front velocity is dictated by a competing mechanism between the exothermic heat (H_e) and the maximum temperature (T_{max}). At a lower PI content of 0.3 wt%, the exothermic heat produced in the dog-bone specimen is relatively lower than that in the flat beam specimen, which resulted in a slightly higher front velocity. As the PI content increases to 0.4 wt% and 0.5 wt %, the front temperature begins to play a more significant role, as evidenced by the higher front temperature observed in the flat beam specimens which exhibited a higher front velocity.

3.2.2. Degree of cure

The degree of cure in dog-bone specimens is compared to that in the flat beam specimens in Fig. 5(d). It can be observed that the dog-bone specimens exhibited consistently higher degree of cure when compared to the flat beam specimens at varying PI weight contents. Specifically, they are 11 %, 9 %, and 7 % higher in the dog-bone specimens as opposed to the flat beam specimens at PI contents of 0.3 wt%, 0.4 wt%, and 0.5 wt%, respectively. Although the front temperature in the dog-bone specimens is consistently lower than that in flat beam specimens (as shown in Fig. 5(b)), the resulting degree of cure is not only governed by the front temperature, but also the geometry and the size of the specimen. For dog-bone specimens, the generated exothermic heat is more constrained in a relatively smaller volume and hence, leading to the improvement of the overall degree of cure.

3.2.3. Tensile properties

A comparison of the tensile properties between the dog-bone specimens and the flat beam specimens is presented in Fig. 6(a) and (b). Note that although the epoxy specimens fabricated in the flat beam shaped cavity is named as flat beam specimens, they were cut into the dog-bone specimens prior to the tensile tests. For the specimens fabricated in the dog-bone shaped cavity, they were directly used in the tensile tests. As shown in Fig. 6(a), initially at a PI of 0.3 wt%, the tensile strength of the dog-bone specimen is about 10 % lower than that of the flat beam specimen. However, as the PI content increases, the tensile strengths of the dog-bone specimens quickly surpass those of the flat beam specimens. In particular, they are 28 % and 124 % higher as the PI content increases to 0.4 wt% and 0.5 wt%, respectively. This could be due to the increased porosity in the flat beam specimens as the PI content increases (seeFig. 4(a)), which is caused by the higher amount of exothermic heat generated in flat beam specimens. Fig. 6(a) also compares the tensile strength of the dog-bone and flat beam specimens fabricated using the traditional oven curing method. It was observed that the neither the traditional dog-bone nor the flat beam specimens exhibit any visible air pores in the epoxy specimen. Hence, these specimens were not affected by the generation of the large amount of air pores. The flat beam traditional specimens showed an identical tensile strength with than that of the dog-bone traditional specimens, which is expected since the geometry of the same material should not affect the tensile strength.

On the other hand, Fig. 6(b) shows the comparison for the tensile modulus. The dog-bone specimens exhibited consistently lower modulus when compared to those flat beam specimens. In particular, they are about 26 %, 2 %, and 18 % lower at PI contents of 0.3 wt%, 0.4 wt%, and 0.5 wt%, respectively. This along with the generally higher tensile strength of the dog-bone specimens, indicates that the dog-bone specimens are more ductile than the flat beam specimens. For the traditional flat beam and dog-bone specimens, no noticeable difference in the tensile modulus has been observed, as expected.

Overall, our results suggest that the FP process and the resulting mechanical properties of the epoxy resin specimens are highly sensitive to the geometry in which the front was initiated and propagated. A geometry that gives a smaller volume results in the generation of a lower total exothermic heat, and thus lower porosity and higher strength. A geometry that gives a larger volume results in the generation of a higher total exothermic heat, and hence a higher degree of cure and a higher modulus in general.

4. Conclusion

In this study, we investigated the UV-induced frontal polymerization (FP) of epoxy resin and delved into the effects of the weight content of the photoinitiator (PI), the UV light intensity, and the specimen geometry (*i.e.,* flat beam *vs.* dog bone) on both the characteristics of the FP and the resulting mechanical properties of neat epoxy specimens. The study mainly leads to the following findings:

The front velocity, front temperature, and the degree of cure increase as the weight content of the photoinitiator (PI) and the UV light intensity

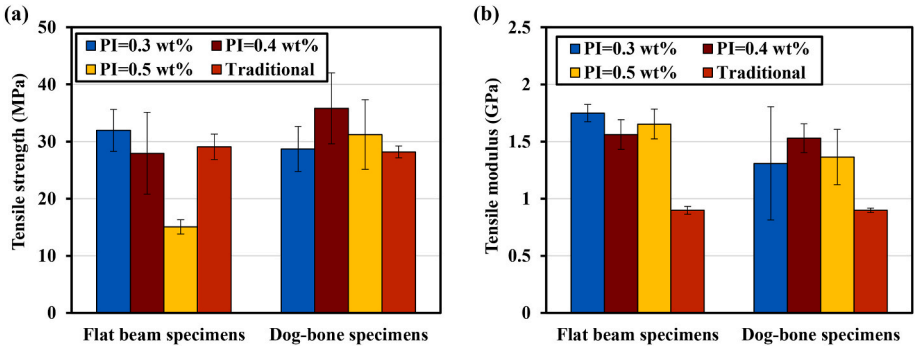

Fig. 6. A comparison of **(a)** tensile strength and **(b)** tensile modulus between flat beam and dog-bone epoxy specimens fabricated at varying PI content under the 15 % UV condition.

increase due to the increased amount of exothermic heat generated in the FP process. Notably, the degree of cure increased from 76 % to 95 % as the PI weight content increases from 0.2 wt% to 0.4 wt% under the UV light with an intensity of 82 mW/cm^2. However, although increasing the PI content and the UV light intensity increases the degree of cure, if the temperature gets overly high, it can cause adverse effect on the tensile and flexural strengths due to the polymer degradation. In our flat beam specimens, the tensile strength dropped by 50 % as the PI content increased from 0.4 wt% to 0.5 wt% while the flexural strength decreased by 24 % as the PI content increased from 0.3 wt% to 0.5 wt%, under the UV light with an intensity of 42 mW/cm^2.

Additionally, the specimen geometry (flat beam *vs.* dog-bone) significantly affects the FP process and the mechanical properties. A geometry that gives a slender gauge section will constrict the heat flow and reduce the heat loss to the ambient environment, and hence improve the degree of cure. Generally, using a geometry with a uniform cross section results in the generation of a higher total exothermic heat, and hence higher front temperature, front velocity, and higher modulus, when compared to the geometry having a slender gauge section. Using the geometry with the slender gauge section results in the generation of a lower total exothermic heat, and hence lower porosity, higher strength, and higher ductility.

Lastly, when compared with epoxy resin specimens cured using the traditional oven curing method, the curing time reduced from 15 h to only less than 1.5 min using the UV-induced FP method. The tensile and flexural strengths of frontal polymerized epoxy resin specimens are comparable and even higher than those of the traditional specimen. This demonstrates the great promise of the UV-induced FP for achieving the in-situ curing of epoxy resin with excellent mechanical properties, which paves the avenue for the efficient and additive manufacturing and repair of thermoset and thermoset based fiber composites.

CRediT authorship contribution statement

Amirreza Tarafdar: Writing – review & editing, Methodology, Investigation, Formal analysis, Data curation. **Wenhua Lin:** Writing – review & editing, Investigation, Formal analysis. **Ali Naderi:** Investigation, Formal analysis. **Xinlu Wang:** Investigation, Formal analysis, Data curation. **Kun (Kelvin) Fu:** Writing – review & editing, Visualization. **Ian D. Hosein:** Writing – review & editing, Supervision, Methodology. **Yeqing Wang:** Writing – original draft, Supervision, Project administration, Methodology, Investigation, Funding acquisition, Formal analysis, Data curation.

Declaration of competing interest

The authors declare that they have no known competing financial interests or personal relationships that could have appeared to influence the work reported in this paper.

Data availability

Data will be made available on request.

Acknowledgments

A. Tarafdar, W. Lin, A. Naderi, I. Hosein, and Y. Wang would like to acknowledge the financial support from National Science Foundation under Award No. CMMI-2208130 and under Award No. CMMI-2202737. The authors thank Mr. Arun Poudel (Graduate Assistant) and Dr. Pranav Soman (Associate Professor) in the Department of Biomedical and Chemical Engineering at Syracuse University for their support and assistance in the high-resolution optical microscopy imaging process.

Appendix A. Supplementary data

Supplementary data to this article can be found online at https://doi.org/10.1016/j.coco.2024.101832.

References

[1] CYCOM® 977-2 and 977-2A Prepreg Technical Data Sheet, URL: https://www.solvay.com/en/product/cycom-977-2. 2016.
[2] K. Button, Out-of-oven curing, Aero. Am. 58 (2) (2020) 14–17.
[3] B. Shi, Y. Shang, P. Zhang, S. Liu, S. Huang, B. Sun, et al., Rapid electrothermal-triggered flooded thermoset curing for scalable carbon/polymer composite manufacturing, Compos. Sci. Technol. 200 (2020) 108409.
[4] O. Uitz, P. Koirala, M. Tehrani, C.C. Seepersad, Fast, low-energy additive manufacturing of isotropic parts via reactive extrusion, Addit. Manuf. 41 (2021) 101919, https://doi.org/10.1016/j.addma.2021.101919.
[5] J. Staal, E. Smit, B. Caglar, V. Michaud, Thermal management in radical induced cationic frontal polymerisation for optimised processing of fibre reinforced polymers, Compos. Sci. Technol. 237 (2023) 110009, https://doi.org/10.1016/j.compscitech.2023.110009.
[6] K. Deng, C. Zhang, K.K. Fu, Additive manufacturing of continuously reinforced thermally curable thermoset composites with rapid interlayer curing, Compos. B Eng. 257 (2023) 110671.
[7] H. Zhang, K. Zhang, A. Li, L. Wan, C. Robert, C.M. Ó Brádaigh, et al., 3D printing of continuous carbon fibre reinforced powder-based epoxy composites, Compos. Commun. 33 (2022) 101239, https://doi.org/10.1016/j.coco.2022.101239.
[8] E. Goli, I.D. Robertson, H. Agarwal, E.L. Pruitt, J.M. Grolman, P.H. Geubelle, et al., Frontal polymerization accelerated by continuous conductive elements, J. Appl. Polym. Sci. 136 (17) (2019) 47418.
[9] A. Stiles, W. Kobler, P. Yeole, U. Vaidya, Photopolymer formulation towards large scale additive manufacturing of autoclave capable tooling, Addit. Manuf. 50 (2022) 102571, https://doi.org/10.1016/j.addma.2021.102571.
[10] S. Lee, Y. Kim, D. Park, J. Kim, The thermal properties of a UV curable acrylate composite prepared by digital light processing 3D printing, Compos. Commun. 26 (2021) 100796.
[11] Y. Ming, Z. Xin, J. Zhang, Y. Duan, B. Wang, Fabrication of continuous glass fiber-reinforced dual-cure epoxy composites via UV-assisted fused deposition modeling, Compos. Commun. 21 (2020) 100401.
[12] J.A. Pojman, V.M. Ilyashenko, A.M. Khan, Free-radical frontal polymerization: self-propagating thermal reaction waves, J. Chem. Soc., Faraday Trans. 92 (16) (1996) 2825–2837, https://doi.org/10.1039/FT9969202825.
[13] Wang Y, Lampkin S. Rapid curing of epoxy resin using self-sustained frontal polymerization towards the additive manufacturing of thermoset fiber composites. In Proceeding of the 37th Annual American Society for Composites Technical Conference. Tucson, Arizona, September 19-21, 20222022. DOI: 10.12783/asc37/36414.
[14] T.Y. Wong, T. Yu, F. Zou, Effect of curing condition on the piezoresistivity of multi-walled carbon nanotube/epoxy nanocomposites, Compos. Commun. 39 (2023) 101557, https://doi.org/10.1016/j.coco.2023.101557.
[15] A. Tarafdar, C. Woodbury, A. Naderi, X. Wang, W. Lin, I.D. Hosein, et al., Mechanical characterization of epoxy resin manufactured using frontal polymerization, in: Proceeding of the American Society for Composites 38th Technical Conference, 2023, https://doi.org/10.12783/asc38/36607. Greater Boston, MA, September 17-20.
[16] B.R. Groce, D.P. Gary, J.K. Cantrell, J.A. Pojman, Front velocity dependence on vinyl ether and initiator concentration in radical-induced cationic frontal polymerization of epoxies, J. Polym. Sci. 59 (15) (2021) 1678–1685.
[17] A. Tarafdar, C. Jia, W. Hu, I.D. Hosein, K.K. Fu, Y. Wang, Three-dimensional modeling of frontal polymerization for rapid, efficient, and uniform thermoset composites manufacturing, Compos. B Eng. 266 (2023) 111029.
[18] Y. Wang, Modeling the through-thickness frontal polymerization of unidirectional carbon fiber thermoset composites: effect of microstructures, J. Appl. Polym. Sci. 139 (31) (2022) e52735.
[19] A. Mariani, S. Fiori, Y. Chekanov, J.A. Pojman, Frontal ring-opening metathesis polymerization of dicyclopentadiene, Macromolecules 34 (19) (2001) 6539–6541, https://doi.org/10.1021/ma0106999.
[20] P.J. Centellas, M. Yourdkhani, S. Vyas, B. Koohbor, P.H. Geubelle, N.R. Sottos, Rapid multiple-front polymerization of fiber-reinforced polymer composites, Compos. Appl. Sci. Manuf. 158 (2022) 106931, https://doi.org/10.1016/j.compositesa.2022.106931.
[21] I.D. Robertson, M. Yourdkhani, P.J. Centellas, J.E. Aw, D.G. Ivanoff, E. Goli, et al., Rapid energy-efficient manufacturing of polymers and composites via frontal polymerization, Nature 557 (7704) (2018) 223–227.
[22] I.D. Robertson, L.M. Dean, G.E. Rudebusch, N.R. Sottos, S.R. White, J.S. Moore, Alkyl phosphite inhibitors for frontal ring-opening metathesis polymerization greatly increase pot life, ACS Macro Lett. 6 (6) (2017) 609–612, https://doi.org/10.1021/acsmacrolett.7b00270.
[23] F.-L. Jin, X. Li, S.-J. Park, Synthesis and application of epoxy resins: a review, J. Ind. Eng. Chem. 29 (2015) 1–11.
[24] A. Tarafdar, G. Liaghat, H. Ahmadi, O. Razmkhah, S.C. Charandabi, M.R. Faraz, et al., Quasi-static and low-velocity impact behavior of the bio-inspired hybrid Al/GFRP sandwich tube with hierarchical core: experimental and Numerical Investigation, Compos. Struct. 276 (2021) 114567.

[25] S. Yang, T. Li, Y. Wang, X. Zhang, S. Wang, J. Huang, et al., Sustainable epoxy composites with high thermal conductivity using poly(lipoic acid) modified liquid metal as crosslinkers, Compos. Commun. 44 (2023) 101747, https://doi.org/10.1016/j.coco.2023.101747.
[26] A. Mariani, S. Bidali, S. Fiori, M. Sangermano, G. Malucelli, R. Bongiovanni, et al., UV-ignited frontal polymerization of an epoxy resin, J. Polym. Sci. Polym. Chem. 42 (9) (2004) 2066–2072.
[27] D. Bomze, P. Knaack, T. Koch, H. Jin, R. Liska, Radical induced cationic frontal polymerization as a versatile tool for epoxy curing and composite production, J. Polym. Sci. Polym. Chem. 54 (23) (2016) 3751–3759, https://doi.org/10.1002/pola.28274.
[28] A.D. Tran, T. Koch, P. Knaack, R. Liska, Radical induced cationic frontal polymerization for preparation of epoxy composites, Compos. Appl. Sci. Manuf. 132 (2020) 105855, https://doi.org/10.1016/j.compositesa.2020.105855.
[29] P. Lepcio, J. Daguerre-Bradford, A.M. Cristadoro, M. Schuette, A.J. Lesser, Frontally polymerized foams: thermodynamic and kinetical aspects of front hindrance by particles, Mater. Horiz. 10 (8) (2023) 2989–2996, https://doi.org/10.1039/D2MH01553F.
[30] B.A. Suslick, J. Hemmer, B.R. Groce, K.J. Stawiasz, P.H. Geubelle, G. Malucelli, et al., Frontal polymerizations: from chemical perspectives to macroscopic properties and applications, Chem. Rev. 123 (6) (2023) 3237–3298, https://doi.org/10.1021/acs.chemrev.2c00686.
[31] K. Yang, Y. Liu, Z. Zheng, Z. Tang, X. Chen, Controlled polymerization and side reaction mechanism of bio-sourced pentanediamine-derived semi-aromatic copolyamides, Polym. Chem. 14 (19) (2023) 2390–2404, https://doi.org/10.1039/D3PY00102D.
[32] ASTM D638-14, Standard Test Method for Tensile Properties of Plastics, ASTM International, 2015.
[33] A. Kumar, Y. Gao, P.H. Geubelle, Analytical estimates of front velocity in the frontal polymerization of thermoset polymers and composites, J. Polym. Sci. 59 (11) (2021) 1109–1118, https://doi.org/10.1002/pol.20210155.